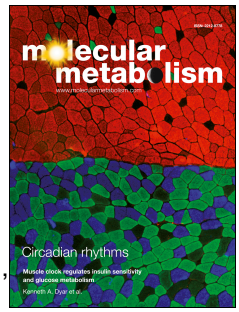

Metabolic insights from a GHSR-A203E mutant mouse model

Lola J. Torz, Sherri Osborne-Lawrence, Juan Rodriguez, Zhenyan He, María Paula Cornejo, Emilio Román Mustafá, Chunyu Jin, Natalia Petersen, Morten A. Hedegaard, Maja Nybo, Valentina Martínez Damonte, Nathan P. Metzger, Bharath K. Mani, Kevin W. Williams, Jesica Raingo, Mario Perello, Birgitte Holst, Jeffrey M. Zigman

PII: S2212-8778(20)30078-8

DOI: https://doi.org/10.1016/j.molmet.2020.101004

Reference: MOLMET 101004

To appear in: *Molecular Metabolism*

Received Date: 8 March 2020

Revised Date: 13 April 2020

Accepted Date: 16 April 2020

Please cite this article as: Torz LJ, Osborne-Lawrence S, Rodriguez J, He Z, Cornejo MP, Mustafá ER, Jin C, Petersen N, Hedegaard MA, Nybo M, Damonte VM, Metzger NP, Mani BK, Williams KW, Raingo J, Perello M, Holst B, Zigman JM, Metabolic insights from a GHSR-A203E mutant mouse model, *Molecular Metabolism*, https://doi.org/10.1016/j.molmet.2020.101004.

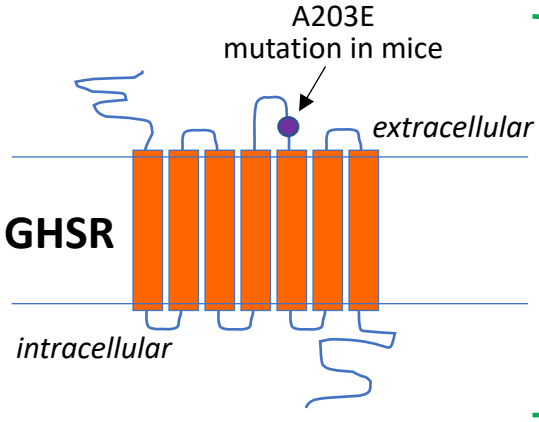

- ✓ ablates constitutive GHSR activity
- ✓ hyperpolarizes arcuate NPY neurons
- ✓ does not affect ghrelin-induced GHSR activity *in vitro* or *ex vivo*
- ✓ prevents ghrelin-induced food intake
- ✓ attenuates ghrelin-induced GH release
- ✓ blunts GH response to severe caloric restriction
- ✓ causes older mice to attain less body length
- ✓ causes older mice to attain less body weight

Metabolic insights from a GHSR-A203E mutant mouse model

Lola J. Torz[1,5], Sherri Osborne-Lawrence[2], Juan Rodriguez[2], Zhenyan He[2], María Paula Cornejo[3], Emilio Román Mustafá[4], Chunyu Jin[1], Natalia Petersen[1], Morten A. Hedegaard[1], Maja Nybo[5], Valentina Martínez Damonte[4], Nathan P. Metzger[2], Bharath K. Mani[2], Kevin W. Williams[2], Jesica Raingo[4], Mario Perello[3], Birgitte Holst[1,5,*] and Jeffrey M. Zigman[2,*]

[1]Department of Biomedical Sciences, University of Copenhagen, Copenhagen, Denmark
[2]Center for Hypothalamic Research, Department of Internal Medicine, UT Southwestern Medical Center, Dallas, Texas, U.S.A.
[3]Laboratory of Neurophysiology and [4]Laboratory of Electrophysiology of the Multidisciplinary Institute of Cell Biology [Argentine Research Council (CONICET) and Scientific Research Commission, Province of Buenos Aires (CIC-PBA)], La Plata, Buenos Aires, Argentina
[5]Section for Metabolic Receptology and Gut-Brain signaling, Novo Nordisk Foundation Center for Basic Metabolic Research, University of Copenhagen, Copenhagen, Denmark

*co-corresponding authors

Correspondence:
Birgitte Holst, MD, PhD
Blegdamsvej 3B,
2100-Copenhagen
Denmark
Tel:+45 21487699
Email:holst@sund.ku.dk

Jeffrey M. Zigman, MD, PhD
5323 Harry Hines Blvd
Dallas, TX 75390-9077
Tel +1 214 648-8621
Email jeffrey.zigman@utsouthwestern.edu

Highlights

Disclosure. The authors report no conflicts of interest in this work.

Abstract

Objective:
Binding of ghrelin to its receptor, growth hormone secretagogue receptor (GHSR) stimulates GH release, induces eating, and raises blood glucose. These processes also may be influenced by constitutive (ghrelin-independent) GHSR activity, as suggested by the findings of short stature in people with the naturally-occurring GHSR-A204E mutation and reduced food intake and blood glucose in rodents administered GHSR inverse agonists, both of which impair constitutive GHSR activity. Here, we aimed to more fully determine the physiologic relevance of constitutive GHSR activity.

Methods:
We generated mice with a GHSR mutation that replaces the alanine at position 203 with glutamate (GHSR-A203E), which corresponds to the above-referenced human GHSR-A204E mutation, and used them to perform *ex vivo* neuronal electrophysiology and *in vivo* metabolic assessments. Also, we measured signaling within COS-7 and HEK293T cells transfected with wild-type GHSR (GHSR-WT) or GHSR-A203E constructs.

Results:
In COS-7 cells, GHSR-A203E resulted in lower baseline IP_3 accumulation than did GHSR-WT; ghrelin-induced IP_3 accumulation was observed for both constructs. In HEK293T cells co-transfected with the voltage-gated $Ca_V2.2$ calcium channel complex, GHSR-A203E had no effect on basal $Ca_V2.2$ current density while GHSR-WT did; both GHSR-A203E and GHSR-WT inhibited $Ca_V2.2$ current in the presence of ghrelin. In cultured hypothalamic neurons from GHSR-A203E and GHSR-deficient mice, native calcium currents were greater than those in neurons from wild-type mice; ghrelin inhibited calcium currents in cultured hypothalamic neurons from both GHSR-A203E and wild-type mice. In brain slices, resting membrane potentials of arcuate NPY neurons from GHSR-A203E mice were hyperpolarized as compared to those from wild-type mice; the same percentage of arcuate NPY neurons from GHSR-A203E and wild-type mice depolarized upon ghrelin exposure. The GHSR-A203E mutation did not significantly affect body weight, body length, or femur length in the first ~6 months of life, yet those parameters were lower in GHSR-A203E mice after 1 yr-of-age. During a 7-d 60% caloric restriction regimen, GHSR-A203E mice lacked the usual marked rise in plasma GH and demonstrated an exaggerated drop in blood glucose. Also, administered ghrelin exhibited reduced orexigenic and GH secretagogue efficacies in GHSR-A203E mice.

Conclusions:
Our data suggest that the A203E mutation ablates constitutive GHSR activity and that constitutive GHSR activity contributes to the native depolarizing conductance of GHSR-expressing arcuate NPY neurons. Although the A203E mutation does not block ghrelin-evoked signaling as assessed using *in vitro* and *ex vivo* models, GHSR-A203E mice lack the usual acute food intake response to administered ghrelin *in vivo*. Also, the GHSR-A203E mutation blunts GH release, and, in aged mice, leads to reduced body length and femur length, which are consistent with the short stature of human carriers of the GHSR-A204E mutation.

Keywords: ghrelin, constitutive activity, growth hormone, GH

1. Introduction

In their seminal paper, Kojima et al. described the identification of ghrelin as an endogenous agonist for GHSR that potently stimulates GH secretion (1). Ghrelin also exerts key orexigenic and glucoregulatory actions, the latter of which prevent life-threatening hypoglycemia in starvation-like settings (2, 3). While binding of ghrelin to GHSR is required for ghrelin action, GHSR signaling also occurs via a ghrelin-independent, constitutive manner (3-7). As first reported in 2003, transient transfection of cultured cells with increasing amounts of human GHSR dose-dependently increases signaling via the Gαq/phospholipase C pathway, raising inositol phosphate (IP) accumulation and inducing cAMP response element-dependent activity (8). These *in vitro* indications of high constitutive GHSR activity have been extended to other signaling systems including reduced β-arrestin recruitment and those involving voltage-gated $Ca_V2.2$ calcium channels, among others (9-14). Indeed, transfection with GHSR increases basal signaling above mock-transfected cells to approximately 50% of GHSR's maximal signaling capacity (13).

Of interest, studies with administered GHSR inverse agonists, which are defined as such by their capacity to inhibit constitutive GHSR activity, suggest physiologically significant effects of constitutive GHSR activity. For example, infusion in rats of the high potency GHSR inverse agonist [D-Arg^{1}, D-Phe^{5}, D-Trp^{7,9}, Leu^{11}]-substance P (8) decreased food intake and body weight (15). Intrarenal infusion of the same compound prevented hypertension in uninephrectomized Dahl salt-sensitive rats fed high fat diet (16). Administration of the GHSR inverse agonist K-(D-1-Nal)-FwLL-NH_2, but not administration of the GHSR antagonists [D-Lys-3]-GHRP-6 or JMV2959, reduced compensatory hyperphagia following a 48 h fast and binge-like high-fat intake in mice (17, 18). Administration of the GHSR inverse agonists GHSR-IA1 and/or GHSR-IA2 reduced food intake and increased energy expenditure in lean C57BL/6N mice, reduced food intake, body weight, and blood glucose in diet-induced obese C57BL/6J mice, and improved oral glucose tolerance in Zucker diabetic fatty rats (19). Also, the GHSR inverse agonist PF-05190457 decreased postprandial blood glucose and delayed gastric emptying in human subjects, although it also blocked administered ghrelin-induced GH secretion (20). This latter finding is a reminder that most inverse agonists also act as antagonists, and furthermore, that many pharmacologic GHSR ligands exhibit differential functional signaling and downstream signaling bias (12, 21-23).

Also suggesting a potentially important physiological role for constitutive GHSR activity, liver-enriched antimicrobial peptide-2 (LEAP2) was recently identified as a second endogenous GHSR ligand – one with both GHSR antagonist and inverse agonist activities (24-27). As such, LEAP2 not only blocks ghrelin-induced GHSR signaling *in vitro*, ghrelin-induced membrane depolarization of arcuate NPY neurons, and ghrelin-induced food intake and GH secretion, but also reduces constitutive IP accumulation in GHSR-transfected cells and hyperpolarizes arcuate NPY neurons (24-27). It has been proposed that LEAP2's actions as a GHSR antagonist and inverse agonist become pronounced when its plasma levels rise, as occurs in obesity, especially postprandially (24, 26).

Notably, a naturally-occurring GHSR mutation that impairs constitutive GHSR activity was reported by Pantel et al (28). This GHSR-A204E mutation, which was identified in two unrelated Moroccan families, segregated with short stature in a dominant manner with a penetrance of ~70% (21, 28). *In vitro* studies revealed that the GHSR-A204E mutant exhibited markedly reduced basal Gαq-mediated signaling, a near total reduction in β-arrestin recruitment, and resistance to the usual signaling effects of [D-Arg^{1}, D-Phe^{5}, D-Trp^{7,9}, Leu^{11}]-substance P, all of which suggest lost constitutive GHSR activity (14, 21, 28). Yet, ghrelin binding and ghrelin-

induced Gαq-coupled signaling were unaltered in GHSR-A204E-transfected cells (28). Thus, the short stature associated with the GHSR-A204E mutation was attributed to lost constitutive GHSR activity (21, 28). Interestingly, several family members carrying the GHSR-A204E mutation also exhibited overweight or obesity (28), and another study independently reported the GHSR-A204E mutation in a child with obesity (29). Other naturally-occurring GHSR mutations causing decreased constitutive GHSR activity and short stature have since been described (21, 29, 30). In the current study, we set out to further investigate the physiological significance of constitutive GHSR activity by introducing an A203E mutation (the mouse correlate of the above-described human GHSR-A204E mutation) into the mouse GHSR sequence.

2. Materials and Methods

2.1. Signaling studies in COS-7 cells

In Copenhagen, COS-7 cells (ATCC®, Wesel Germany) were grown in Dulbecco's modified Eagle's medium (DMEM) 1885 containing 10% fetal bovine serum (FBS), 2 mM L-glutamine, and 1% penicillin/streptomycin at 37°C in a 10% CO_2 incubator. Cells seeded at a density of 20,000 cells/well in a 96-well plate were transiently transfected with 0.4 µg of pCMV-Tag2B plasmid (Stratagene, La Jolla) DNA per well by calcium phosphate precipitation, using a method modified from (31). The plasmids contained either GHSR-WT or GHSR-A203E constructs, which were generated using the PCR overlap extension method with Pfu polymerase (Promega, Waltham) as previously described (14). The sequences of the constructs were verified by DNA sequencing (Eurofins MWG Operon, Ebersberg). Five hrs after transfection, the medium was exchanged for growth medium (Dulbecco's modified Eagle's medium (DMEM) 1885 containing 10% fetal bovine serum (FBS), 2 mM L-glutamine, and 1% penicillin/streptomycin) containing 5 µL/mL of *Myo*-[2-^{3}H(N)]-inositol (Perkin Elmer, Skovlunde), and the cells were incubated for 2 d. Signaling studies were performed by removing the medium, washing the cells once with 1x HBSS buffer, and then incubating at 37°C in 100 µL HBSS buffer containing 10mM LiCl), and a range of different ghrelin (Polypeptide, Inc., Hillerød) concentrations. After a 90 min incubation, the cells were placed on ice, lysed with ice cold 10 mM formic acid for at least 30 min, transferred to 96-well plates containing SPA-YSI beads (Perkin Elmer), shaken at full speed on a plate shaker (Perkin Elmer) for at least 10 min, centrifuged for 5 min at 1500 rpm, and incubated for 4 hr at room temperature. IP_3 accumulation was measured using a Microbeta (Perkin Elmer). For each replicate, the Emax values of the GHSR-WT construct were normalized and set to 100% for further analysis.

2.2. Whole-cell patch-clamp in HEK293T cells

In La Plata, HEK293T cells (kindly provided by Dr. Diane Lipscombe, Brown University, Providence) were grown in DMEM (Gibco Thermo Fisher Scientific, Waltham) containing 10% FBS (Internegocios, Mercedes). Cells were transiently transfected with plasmids containing GHSR-WT or GHSR-A203E and plasmids containing voltage-gated calcium channel subunits CaV2.2 (Cacna1b, GenBank access # AF055477) with auxiliary subunits CaVβ3 (Cacnb3, GenBank access # M88751) and CaVα2δ1 (Cacna2d1, GenBank access # AF286488), using Lipofectamine 2000 (Invitrogen). CaV subunits were kindly provided by Dr. Lipscombe and GHSR-WT was kindly provided by Dr. Jacky Marie, Université de Montpellier, France). The GHSR-A203E construct was generated through directed mutagenesis of a mouse GHSR (MC212500, Origene, Rockville)-containing plasmid by Dr. Silvia Rodriguez at the IMBICE, La Plata. For experiments lacking one or more plasmids, cells were transfected with empty plasmid pcDNA3.1 (+) (Invitrogen) to maintain an equivalent total cDNA amount in the transfection mix and an eGFP-containing plasmid to identify transfected cells. After transfection, cells were cultured for 24 h, dispersed with 0.25 mg/mL trypsin, rinsed twice in DMEM, and kept at room temperature in DMEM for whole-cell patch-clamp recordings. Internal pipette solution

contained (in mM): 134 CsCl, 10 EGTA, 1 EDTA, 10 HEPES and 4 MgATP (pH 7.2 with CsOH). External solution contained (in mM): 2 $CaCl_2$, 1 $MgCl_2$, 10 HEPES and 140 choline chloride (pH 7.4 with CsOH). Cells were held at -100 mV to remove closed-state inactivation (32). The test-pulse protocol consisted of square pulses applied from -100 to +10 mV every 10 s. Electrophysiological recordings were acquired using an Axopatch 200 amplifier (Molecular Devices). Data were sampled at 20 kHz and filtered at 10 kHz (−3 dB) using PCLAMP8.2 software (Molecular Devices). Recording electrodes with resistances between 2 and 5 MΩ were used and filled with internal solution. Series resistances less of 6 MΩ were admitted and compensated to 80 % with a 10 μs lag time. Current leak was subtracted on-line using a P/−4 protocol. All recordings were obtained at room temperature (23°C).

2.3. Generation of GHSR-A203E and GHSR-A203E-null mouse lines

The targeting construct used to generate our previously-reported GHSR-null mouse line (33), which contains a *loxP*-flanked transcriptional blocking cassette (TBC) within an intron located downstream of the transcriptional start site and upstream of the translational start site of the mouse *Ghsr* gene, surrounded by *Ghsr* homology arms, was mutated using site-directed mutagenesis (QuickChange II XL Site-Directed Mutagenesis Kit, Agilent, Santa Clara). Plasmid containing the GHSR-null targeting construct was amplified by PCR using primers containing the desired mutation (underlined) at the codon for amino acid 203 [5'-GCCACCGAGTTCGAAGTGCGCTCTGGGC-3' and its reverse complement], digested with *DpnI, and* transformed into Top10 one shot competent cells (Agilent). DNA from the resulting clones was sequenced to confirm successful introduction of only the desired mutation. The resulting GHSR-A203E plasmid was submitted to the UT Southwestern Medical Center Transgenic Core Facility for gene targeting. Correctly targeted ES cell clones were identified by Southern blot and PCR analyses, as done originally for the GHSR-null line (1). Two ES cell clones were sequenced to confirm presence of the desired mutation and then sent for blastocyst injection. Germline transmission was established for both clones and the resulting mice were backcrossed once to C57Bl/6N. GHSR-A203E-null mice (harboring 2 copies of the *Ghsr* allele containing the *loxP*-flanked TBC + the A203E mutation) and their littermates, which included wild-type mice (harboring 2 copies of the wild-type *Ghsr* allele) and heterozygotes, were viable and were born with the expected Mendelian distribution upon mating of heterozygotes, as confirmed by both Southern blot analysis of genomic DNA and by sequencing (data not shown).

Mice heterozygous for the GHSR-A203E-null allele from the initial backcross to C57Bl/6N were crossed to Zona Pellucida 3 (ZP3-cre) mice (34) to generate female breeders with one copy of the GHSR-A203E-null allele and one copy of the ZP3-cre transgene. As the ZP3-cre removes the TBC from the ova of the female breeders, when crossed to C57Bl/6N males, they result in progeny with one copy of the GHSR-A203E allele (the GHSR-A203E-null allele minus one *loxP* site and the TBC) and one copy of the ZP3-cre allele. Subsequent crosses to C57Bl/6N were done to remove ZP3-Cre. Finally, mice heterozygous for the GHSR-A203E allele were crossed to each other to generate GHSR-A203E mice (harboring 2 copies of the *Ghsr* allele containing the A203E mutation) and their littermates, which included wild-type mice and heterozygotes. Study mice were derived from heterozygotes that had been backcrossed onto C57Bl/6N for 7 generations.

2.4. Mouse studies: general

Ex vivo studies were performed using tissues taken from mice housed in La Plata (Figure 3) and in Dallas (Figure 4). *In vivo* studies were performed in Dallas (Figure 5, 7A, 8) and Copenhagen (Figure 2B, 2C, 6, 7B-7G). Mice were housed at room temperature (Dallas: 21.5-22.5ºC; Copenhagen: 22ºC ± 2ºC; La Plata: 23ºC) using a 12 h light-dark cycle and were provided *ad lib* access to water and standard chow [Dallas: 2016 Teklad Global 16% Protein Rodent Diet

(Envigo, Indianapolis); Copenhagen: Altromin 1314 (extruded form, Altromin GmbH & Co. KG, Im Seelenkamp); La Plata: Gepsa Feeds (Grupo Pilar, Pilar, Argentina)], except as noted. Animal procedures were approved by the Institutional Animal Care and Use Committee of UT Southwestern Medical Center, the Danish Working Environment Authority at University of Copenhagen, or the Institutional Animal Care and Use Committee of the IMBICE.

2.5. Whole-cell patch-clamp in cultured hypothalamic neurons

In La Plata, hypothalamic neuronal cultures were derived from GHSR-A203E, GHSR-A203E-null, and wild-type mice at embryonic days 16–18, as described in (35). Hypothalami were removed from embryonic brains, placed in sterile Hanks' solution and rinsed twice. Cells were dissociated with 0.25 mg/mL trypsin (Microvet, Buenos Aires) at 37°C for 20 min, after which 300 µL of fetal bovine serum (FBS, Internegocios) and 0.28 mg/mL deoxyribonuclease I (Sigma-Aldrich, Buenos Aires) were added. The cells were mechanically dissociated using several glass pipettes with consecutively smaller diameter tips. ~70,000 cells were plated on 12 mm-diameter glass coverslips treated with poly-L-lysine (Sigma-Aldrich) and laid over 24-well plates. Cells were incubated at 37°C in a 95% air/5% CO_2 atmosphere with DMEM/F12 (Microvet) 1:1 medium supplemented with B27 supplement (1:50, Gibco, Thermo Fisher Scientific), 10% FBS, 0.25% glucose, 2 mM glutamine (Gibco), 3.3 µg/mL insulin (Novo Nordisk Pharmaceutical Industries, Inc., Buenos Aires), 40 µg/mL gentamicin sulfate salt (Richet, Buenos Aires), and 1% vitamin solution (Microvet). On the fourth day in culture, half the incubating medium was replaced with fresh medium containing cytosine *β*-D-arabinofuranoside (Sigma-Aldrich) to reach a final concentration of 5 µM.

Barium currents of primary neuronal cultures were obtained following 7–15 days of culture. The neurons were patched in voltage-clamp whole-cell mode at a holding potential of -80 mV, applying squared test pulses to 0 mV for 20 ms every 10 s. (36). Internal pipette solution contained (mM): 134 CsCl, 10 EGTA, 1 EDTA, 10 HEPES, and 4 MgATP, pH 7.2 with CsOH. Neurons were bathed with high sodium external solution containing (mM): 135 NaCl, 4.7 KCl, 1.2 $MgCl_2$, 2.5 $CaCl_2$, 10 HEPES, and 10 glucose, pH 7.4 with NaOH. After getting the whole cell configuration, Ca_V currents were recorded after replacing the external solution with a high barium solution containing (mM): 10 $BaCl_2$, 110 choline chloride, 20 tetraethylammonium chloride, 1 $MgCl_2$, 10 HEPES, 10 glucose, and 0.001 tetrodotoxin (TTX; Sigma-Aldrich), pH 7.4 with CsOH. Electrophysiological recordings were acquired as described above (**2.2**).

2.6. Whole-cell patch-clamp in brain slices

In Dallas, GHSR-A203E mice were crossed to NPY-hrGFP mice [kindly provided by Dr. Joel Elmquist (UT Southwestern Medical Center (37)] to generate GHSR-A203E and wild-type littermates with humanized *Renilla reniformis* green fluorescent protein-labeled NPY neurons. Recordings from NPY-hrGFP neurons within 250 µm-thick coronal hypothalamic slice preparations from 8- to 12-wk-old male mice and data analysis were performed as in (26, 38, 39). The pipette solution for whole-cell recording contained (mmol/L): 120 K-gluconate, 10 KCl, 10 HEPES, 5 EGTA, 1 $CaCl_2$, 1 $MgCl_2$, 2 MgATP, and either 0.03 Alexa Fluor 594 or 0.03 Alexa Fluor 350 hydrazide dye (pH 7.3). Epifluorescence was briefly used to target fluorescent cells, at which time the light source was switched to infrared differential interference contrast imaging to obtain the whole-cell recording (Zeiss Axioskop FS2 Plus equipped with a fixed stage and a QuantEM:512SC electron-multiplying charge-coupled device camera). Electrophysiological signals were recorded using an Axopatch 700B amplifier (Molecular Devices, San Jose), low-pass filtered at 2–5 kHz, and analyzed offline on a PC with pCLAMP programs (Molecular Devices). Recording electrodes had resistances of 2.5–5 MΩ when filled with the K-gluconate internal solution. Input resistance was assessed by measuring voltage deflection at the end of the response to a hyperpolarizing rectangular current pulse step (400 ms of −10 to −50 pA).

Ghrelin (rat; 100 nmol/L, Innovagen, Lund; Catalog # SP-GHRL-1) was added to the oxygenated ACSF bathing the hypothalamic slices for specific experiments. Solutions containing ghrelin were typically perfused for 2–4 min. A drug effect was required to be associated temporally with peptide application, and the response had to be stable within a few minutes. A neuron was considered depolarized or hyperpolarized if a change in membrane potential was at least 2 mV in amplitude.

2.5. Long-term feeding studies

Four wk-old mice were individually-housed one wk after weaning. In Dallas (Figure 5), body weight and food intake were monitored weekly at 9:00 am for 21 wks. Cumulative feed efficiency was calculated by comparing body weight at each weekly time point to the starting body weight and then dividing this body weight gain value by the energy content of the chow consumed over the same duration. Nose-to-anus body lengths of female mice were assessed by placing 25 wk-old mice anesthetized with isoflurane prone on a ruler. In Copenhagen (Figure 6), body weights were measured at various time points between the ages of 21 – 66 wks. Body lengths were assessed as above in anesthetized mice at 3 different time points. At 66 wks-of age, femurs and hypothalami were extracted from euthanized mice. Femur lengths were measured using calipers.

2.7. Administered ghrelin-induced food intake

In Dallas (Figure 7A), following the long-term feeding study, the 25 wk-old male mice were handled for 3 days to acclimatize them, after which they were administered s.c. injections of saline, and then 0.1 mg/kg ghrelin 2 d later, followed by 1.0 mg/kg ghrelin 2 d afterwards, at 9:30 am. Two-hr intake of a standard chow pellet placed on the cage floor was determined after each injection. At 26 wks-of-age, the males were anesthetized and nose-to-anus body lengths assessed as above. Femurs extracted from euthanized 26 wk-old mice were measured using calipers. In Copenhagen (Figure 7B-7C), a separate cohort of 9-12 wk-old male mice was individually housed within a 16-chamber indirect calorimetry system (PhenoMaster; TSE Systems, Bad Homburg) after 4 d in an identical set of acclimation cages. The mice received s.c. injections of either ghrelin (Polypeptide, Inc., Hillerød) (2 mg/kg vs. saline in a crossover fashion between 10.30 and 11.00 am, with a 2 d intervening period). Food intake and respiratory exchange ratio (RER) were determined 2 h following the injections.

2.8. Administered ghrelin-induced GH secretion

In Copenhagen, ghrelin- and GHRH-induced GH secretion were assessed in a new cohort of male mice aged 7 and 10 wks, respectively. Fifteen minutes after anesthesia with pentobarbital (i.p. 50 mg/kg body weight), ghrelin (0.5 mg/kg i.p.; Polypeptide, Inc.) or GHRH (0.5 mg/kg i.p.; Phoenix Pharmaceuticals, Karlsruhe) were injected. Blood was sampled from the orbital sinus before and 5 min after injections, as described previously (40, 41).

2.9. 7-d 60% caloric restriction protocol

In Dallas, 7-week-old male mice were individually housed for 1 wk during which time daily food intake was measured for 3 successive days to determine mean usual daily intake for each mouse. Mice were weighed and blood glucose determined from tail nicks using a Contour® Next blood glucose monitoring system (Bayer, Mishawaka) daily, 30 min before lights out. Mice were provided access to 40% of their usual daily calories in the form of their usual diet for 7 d, beginning 15 min before lights out, as described previously (42). Body composition was determined using an EchoMRI (Echo Medical Systems, Houston) at the start of the experiment, and again on days 4 and 6. Blood for GH and ghrelin determinations was collected on days 0, 5, and 7 by quick superficial temporal vein (submandibular) bleed into ice-cold EDTA-coated microtubes immediately after assessing blood glucose.

2.10. Hormone levels

For plasma ghrelin levels, p-hydroxymercuribenzoic acid was added (final concentration 1 mM) to EDTA-treated blood, tubes were centrifuged, and HCl was added (final concentration 0.1N), prior to storage at –80°C. No further processing of the EDTA-treated blood was performed prior to GH or IGF-1 determinations. To measure pituitary GH levels, pituitaries were lysed using RIPA lysis buffer [1% Triton X-100, 150 mM NaCl, 10 mM Tris-HCl (pH 7.5), 1 mM EDTA, 1% NP-40, and complete mini Protease Inhibitor Cocktail; Roche, Mannheim] and homogenized using a Qiagen TissueLyser II (Germantown). Ghrelin, GH, and IGF-1 levels were measured using commercial ELISA kits (EZRGRA-90K, EMD Millipore, Billerica; EZRMGH-45K, EMD Millipore; 22-IG1MS-E01, ALPCO®, Reutlingen). The endpoint calorimetric assays were performed using a PowerWave XS Microplate spectrophotometer and KC4 Junior software (BioTek Instruments, Winooski) or ClarioStar, software version 5.40R2 and Mars software version 3.3 (BMG LabTech, Ortenberg).

2.10. Quantitative PCR

Hypothalamic RNA [from 66 wk-old mice (see above)] and pituitary RNA (from 14 wk-old mice) was extracted using the RNeasy micro kit (Qiagen). RNA concentration was measured using a NanoDrop™ 2000 Spectrophotometer (Thermo Fisher Scientific). RNA samples were reverse transcribed to cDNA using SuperScript™ III Reverse Transcriptase (Thermo Fisher Scientific). The mix was incubated at 25°C for 5 min, 50°C for 60 min, and 70°C for 15 min using Eppendorf Vapo-protect Mastercycler. cDNA sample was diluted 20x in sterile water and stored at -20°C until further analysis. Diluted cDNA sample was mixed with PrecisionPLUS qPCR Master Mix (Primer Design LTd., Southampton) according to the manufacturer's description. Samples were run using a LightCycler® 480 Instrument II (Roche, Basel), LightCycler® 480 software, version 1.5.1.62 and the delta-delta Ct method using GAPDH as housekeeping gene was used to quantify the mRNA expression.

The following PCR primers, designed with Primer 3 (http://bioinfo.ut.ee/primer3-0.4.0/), were used: GHSR (5'-AAGATGCTTGCTGTGGTGGT-3', 5'-AAAGGACACCAGGTTGCAGT-3'), GH (5'-CTACAAAGAGTTCGAGCGTGCCTAC-3', 5'-CAATTCCATGTCGGTTCTCTGCT-3'), UCP2 (5'-CCTACAAGACCATTGCACGA-3', 5'-TGTCATGAGGTTGGCTTTCA-3'), SSTR2 (5'-TTTGACCTCAACGGCTCACT-3', 5'-GCGTTGCTTGTCATGTCGTA-3'), SSTR5 (5'-TGTTCGTGGGCTGCTGGCTG-3', 5'-GGGCTCCTCGGGTAGCGTGA-3'), NPY (5'-TGGACTGACCCTCGCTCTAT-3', 5'-TGTCTCAGGGCTGGATCTCT-3'), POMC (5'-AGAGAGCTGCCTTTCCGCGAC-3', 5'-GCAGGAGGGCCAGCAACAGG-3'), GHRH (5'-CCAATTATATGCCCGCAAAC-3', 5'-GCTGAAAGCTTCATCCTTGG-3'), and GAPDH (5'-AAGGGCTCATGACCACAGTC-3', 5'-GGATGCAGGGATGATGTTCT-3').

2.11. Statistical analyses

Analyses were performed using the tests indicated in the figure legends using GraphPad Prism 6.0 (Graph-Pad Software, San Diego) or NCSS 2007 (NCSS Statistical Software, Kaysville). All data were first subjected to a Grubb's Outlier Test. Data are expressed as mean ± SEM. P-values <0.05 were considered statistically significant, and values $0.05 \leq P < 0.1$ were considered to be evidence of statistical trends.

3. Results

3.1. The GHSR-A203E mutant lacks constitutive GHSR activity but retains ghrelin-dependent GHSR activity in heterologous expression systems

We measured IP_3 accumulation in COS-7 cells transiently transfected with constructs encoding the mouse wild-type GHSR (GHSR-WT) or GHSR-A203E. As shown previously for the corresponding human constructs (14), in the absence of ghrelin, cells expressing GHSR-A203E accumulated less basal IP_3 than cells expressing GHSR-WT (GHSR-A203E: 3.7% vs. GHSR-WT: 44.3% of the maximal response to ghrelin; Figure 1A). Ghrelin dose-dependently increased IP_3 accumulation in both groups, with no significant differences observed at 10^{-6} M or 10^{-5} M ghrelin (Figure 1A). Separately, we recorded calcium currents in HEK293T cells expressing the $Ca_V2.2$ calcium channel complex alone (control) or with GHSR-WT vs. GHSR-A203E. As shown previously for human GHSR-WT (10), in the absence of ghrelin, mouse GHSR-WT reduced $Ca_V2.2$ current density whereas GHSR-A203E did not (Figure 1B, 1C). Ghrelin inhibited $Ca_V2.2$ current in cells co-expressing either GHSR-WT or GHSR-A203E (Figure 1D, 1E). These *in vitro* studies suggest that the A203E mutation eliminates constitutive GHSR activity but still permits ghrelin-dependent GHSR signaling.

3.2. A newly-generated novel GHSR-A203E mouse model expresses GHSR-A203E in place of GHSR-WT

The remaining studies utilized a novel mouse model expressing GHSR-A203E instead of GHSR-WT. To generate these mice, we inserted a *loxP*-flanked transcriptional blocking cassette (TBC) into an intron located downstream of the transcriptional start site and upstream of the translational start site of the mouse *Ghsr* gene. Additionally, we mutated the codon for the alanine at position 203 to encode glutamate. Mice harboring two copies of the GHSR-A203E gene with the upstream loxP-flanked TBC are hereafter referred to as GHSR-A203E-null mice; these mice express neither GHSR-WT nor GHSR-A023E. These mice were crossed with Zp3-Cre mice (34) to remove the TBC. Mice harboring two copies of the GHSR-A203E gene with the TBC deleted are hereafter referred to as GHSR-A203E mice; these mice express GHSR-A203E instead of GHSR-WT (Figure 2A).

RT-PCR analysis of hypothalamic and pituitary glands confirmed similar levels of mRNA encoding GHSR-A203E in GHSR-A203E mice as mRNA encoding GHSR-WT in wild-type littermates (Figure 2B, 2C). RT-PCR analysis of a selected group of food intake- and body weight-related transcripts and GH secretion-related transcripts revealed no effect of the GHSR-A203E mutation on mRNA levels of NPY or uncoupling protein-2 (UCP2) in hypothalami or of growth hormone releasing hormone receptor (GHRHR) or somatostatin receptors 2 or 5 (SSTR2 or SSTR5) in pituitaries (Figure 2B, 2C). Hypothalamic pro-opiomelanocortin (POMC) mRNA expression was increased while pituitary GH mRNA expression was decreased in GHSR-A203E mice (Figure 2B, 2C). Thus, GHSR-A203E mice express GHSR-A203E at levels similar to those of wild-type GHSR in wild-type mice. Furthermore, the GHSR-A203E mutation alters hypothalamic POMC and pituitary GH mRNA expression, without effects on a selected set of related transcripts.

3.3. Cultured hypothalamic neurons from GHSR-A203E mice lack constitutive GHSR activity but retain ghrelin-dependent GHSR activity

We assessed native calcium currents in cultured mediobasal hypothalamic neurons from GHSR-A203E mice, GHSR-A203E-null mice, and wild-type littermates by measuring barium current densities at baseline and in response to ghrelin. This region contains a dense population of arcuate NPY neurons, which represent a well-established site of GHSR expression (43, 44). Barium current densities in GHSR-A203E neurons were similar to those in GHSR-A203E-null neurons but were significantly increased as compared to those in wild-type neurons (Figure 3A,

3B). This increased calcium current within GHSR-A203E-null neurons is similar to that observed in the related GHSR-null model of GHSR deficiency (35). Ghrelin inhibited native calcium current in hypothalamic neurons from both wild-type and GHSR-A203E mice, although it had no effect in neurons from GHSR-A203E-null mice (Figure 3C, 3D). Thus, substitution of GHSR-A203E for wild-type GHSR in hypothalamic neurons that normally express GHSR increases native calcium current (similarly to the effect of GHSR deletion) but maintains the capacity to inhibit calcium current in response to applied ghrelin (similarly to the effect of ghrelin in neurons from wild-type mice).

3.4. Arcuate hypothalamic NPY neurons harboring the GHSR-A203E mutation exhibit hyperpolarized membrane potentials yet retain ghrelin responsivity

We performed whole-cell patch-clamp recordings on two sets of hrGFP-labelled arcuate NPY neurons in brain slices from wild-type and GHSR-A203E littermates (Figure 4A, 4B). GHSR-expressing arcuate NPY neurons depolarize upon ghrelin exposure (43, 44). The first set included 39 wild-type and 38 GHSR-A203E neurons. GHSR-A203E neurons were hyperpolarized as compared to wild-type neurons (wild-type mice: Resting membrane potential = -40 ± 1.1 mV, Input resistance 1.3 ± 0.1 GΩ, Whole-cell capacitance 11.3 ± 0.4 pF vs. GHSR-A203E mice: Resting membrane potential = -46 ± 0.7 mV, Input resistance 1.3 ± 0.1 GΩ, Whole-cell capacitance 11.5 ± 0.5 pF). The second set was tested for ghrelin-induced changes and included 20 wild-type and 15 GHSR-A203E neurons. Ghrelin depolarized 40% of arcuate NPY neurons from both wild-type and GHSR-A203E littermates (Figure 4C-4E). The second set's ghrelin-responsive neurons were hyperpolarized at baseline in GHSR-A203E mice as compared to wild-type mice (wild-type mice: Resting membrane potential = -45 ± 1.3 mV, Input resistance 1.3 ± 0.1 GΩ, Whole-cell capacitance 12.6 ± 0.9 pF vs. GHSR-A203E mice: Resting membrane potential = -49 ± 2.2 mV, Input resistance 1.2 ± 0.1 GΩ, Whole-cell capacitance 11.0 ± 1.0 pF). The lower resting membrane potential in ghrelin-responsive GHSR-A203E neurons likely contributed to their enhanced ghrelin-induced change in membrane potential (Figure 4E). Mean ghrelin-induced action potential frequencies in GHSR-A203E neurons vs. wild-type neurons were similar (data not shown). Thus, constitutive GHSR activity contributes to a native depolarizing conductance in arcuate NPY neurons. Also, ghrelin depolarizes the same percentage of arcuate NPY neurons in GHSR-A203E mice as in wild-type littermates.

In addition, rectangular current steps (400 ms; ±50 pA) were applied to the plasma membranes of the arcuate NPY neurons to obtain current–voltage (I–V) plots. The depolarization was concomitant with a decrease in input resistance (wild-type mice: 38.5%, n=3, 1.3 ± 0.2 GΩ for ACSF control; 0.8 ± 0.1 GΩ for ghrelin, Figure 4F vs. GHSR-A203E mice: 35.7%, n=3, 1.4±0.1 GΩ for ACSF control; 0.9 ± 0.1 GΩ for ghrelin, Figure 4G). Subsequent linear regression analysis revealed the reversal potential of the ghrelin-induced depolarization to be -23 ± 2.7 mV in wild-type mice and -20 ± 4.7 mV in GHSR-A203E mice (Figure 4F, 4G). This suggests that a putative non-selective cation conductance may be involved in the ghrelin-induced depolarization of arcuate NPY neurons (45-47).

3.5. GHSR-A203E mice develop reduced body weight and body length when aged.

We monitored weekly body weights and food intake of individually-housed male and female GHSR-A203E and wild-type littermates with *ad lib* access to regular chow for 21 wks, beginning at 4 wks-of-age. No genotype-dependent differences in body weights were observed over the course of the study (Figures 5A, 5B), although the GHSR-A203E mice gained slightly less body weight (Figures 5C, 5D). Weekly food intake over the course of the study was slightly greater in GHSR-A203E mice (Figures 5E-5H). Cumulative feed efficiency (defined as body weight gain per kilocalories of food consumed) was slightly lower over the course of the study in male

GHSR-A203E mice but not females (Figures 5I, 5J). Body lengths (Figures 5K, 5L) and femur lengths (Figure 5M) at the end of the 21-wk study were genotype-independent.

We also monitored weekly body weights in a second cohort of individually-housed male GHSR-A203E and wild-type littermates with *ad lib* access to regular chow from 21-22 wks-of-age until 65-66 wks-of-age. Although starting body weights of the two genotypes were without a statistically-significant difference, they gradually diverged, leading to lower body weights for the GHSR-A203E mice (Figure 6A). Similarly, although body lengths of the two genotypes were without a statistically-significant difference at 21-22 or 32-33 wks-of age, by 65-66 wks-of-age, GHSR-A203E were shorter in body length (Figure 6B). Femur lengths of the 65-66 wk-old GHSR-A203E mice also were shorter than those from wild-type littermates (Figure 6C).

Thus, while the GHSR-A203E mutation does not affect body weight, body length, or femur length in a statistically-significant manner in the first ~6 mo. of life, it is associated with decreased body weight, body length, and femur length in mice aged > 1 yr. This is despite a slightly increased food intake in younger GHSR-A203E mice, albeit younger male mice also gained slightly less weight per food consumed.

3.6. Orexigenic and GH secretagogue effects of administered ghrelin are blunted in GHSR-A203E mice

We assessed acute food intake responses to administered ghrelin. In a first set of mice (25 wk-old male GHSR-A203E and wild-type littermates individually-housed in their home cages), ghrelin dose-dependently increased 2-h food intake over that induced by saline in wild-type mice but not in GHSR-A203E littermates (Figure 7A). A similar observation was made for ghrelin using a single, higher dose in a second set of mice (9-12 wk-old male GHSR-A203E and wild-type littermates individually-housed in metabolic chambers) (Figure 7B). The corresponding respiratory exchange ratio (RER) values increased in wild-type mice administered ghrelin but not in GHSR-A203E mice (Figure 7C).

We also assessed GH secretion in response to administered ghrelin in GHSR-A203E and wild-type mice littermates. Whereas ghrelin markedly increased plasma GH in wild-type mice as compared to saline, its GH secretagogue efficacy was dramatically reduced (although still present) in GHSR-A203E mice (Figure 7D). In contrast, administered GHRH, which increases GH release in a GHSR-independent manner, increased plasma GH levels in both wild-type and GHSR-A203E mice (Figure 7E).

Also, we measured plasma IGF-1 and pituitary GH content from the above-described cohort of 65-66 wk-old GHSR-A203E and wild-type littermates. Following an overnight fast, plasma IGF-1 was lower while pituitary GH content was higher in GHSR-A203E mice (Figure 7F, 7G).

These data suggest that GHSR-A203E mice are resistant to the usual acute orexigenic and GH secretagogue actions of administered ghrelin. Also, seemingly coinciding with the decreased body length and femur length in aged GHSR-A203E mice, plasma levels of the downstream GH effector IGF-1 were lower although pituitary GH content was higher, suggesting a possible defect in GH release and an ensuing decrease in IGF-1 recruitment in GHSR-A203E mice.

3.7. GHSR-A203E mice submitted to a caloric restriction protocol exhibit a markedly blunted GH response and an exaggerated drop in blood glucose

Finally, we submitted GHSR-A203E and wild-type littermates to a week-long, severe caloric restriction protocol in which mice were provided access to only 40% of their usual daily calories. This protocol induces progressive elevations in plasma GH in wild-type mice but not in ghrelin-

knockout or ghrelin *O*-acyltransferase-knockout mice (48, 49). These rises in GH help prevent the development of life-threatening hypoglycemia that is otherwise observed in mice lacking ghrelin, ghrelin *O*-acyltransferase, GHSR, ghrelin cell β_1-adrenergic receptors, or hepatic GH receptors, mice lacking ghrelin cells, and mice overexpressing LEAP2 (24, 42, 48-53). Over the course of the 7-d regimen, no genotype-dependent differences in body weight or body composition were observed (Figure 8A-8C). Plasma GH rose only in wild-type mice, plasma ghrelin rose in a genotype-independent manner, and a more precipitous drop in blood glucose was noted in the GHSR-A203E mice (Figure 7D-7F). Additionally, although no statistically-significant, genotype-dependent difference in survival was noted, 3 out of 20 of the GHSR-A203E mice died whereas none of the 9 wild-type littermates died (Figure 7G).

4. Discussion

In the current study, we used *in vitro*, *ex vivo*, and *in vivo* methods to assess the physiological significance of constitutive GHSR activity. The study was based on published work using *in vitro* heterologous cell expression systems, which suggested that the naturally-occurring GHSR-A204E mutation associated with short stature in humans impairs constitutive (ghrelin-independent) GHSR activity while retaining ghrelin-dependent GHSR activity. For the current study, we took advantage of the mouse GHSR-A203E correlate of the human GHSR-A204E mutation.

When comparing the phenotype of GHSR-A203E mice to that of human carriers of the GHSR-A204E mutation, similarities in body length and GH deficiency were observed. The human GHSR-A204E mutation is associated with a high penetrance of short stature, which one might assume results from impaired GH secretion due to the mutant GHSR (21, 28). Such was the case in two of the four GHSR-A204E carriers with short stature in whom GH and IGF-1 were reported: a low GH peak and low IGF-1 were observed in one subject and a low GH peak but normal IGF-1 were observed in a second subject; however, the remaining two subjects had normal GH peaks and IGF-1 (28). Three of those subjects received GH treatment, and as a result, increased their growth velocity (28). Reminiscent of the highly penetrant short stature phenotype in the human GHSR-A204E carriers, here we show that GHSR-A203E mutant mice exhibited slight, albeit statistically-significant, reductions in body length and femur length by 65-66 wks-of-age (4.3% and 2.6%, respectively). Differences in these parameters were not observed at 25 wks-of-age, though, which contrasts with the GHSR-A204E-associated growth deficiency in human carriers, which was observed in childhood (28).

Also reminiscent of the GH deficiency observed in at least some of the human GHSR-A204E carriers, plasma IGF-1 was reduced in overnight-fasted 65-66 wk-old GHSR-A203E mice. Additionally, over the course of a 7-d 60% caloric restriction that usually (in wild-type mice) leads to progressive GH elevation, GHSR-A203E mice lacked any substantial increase in GH release. The exaggerated drop in blood glucose observed during the caloric restriction protocol paralleled the life-threatening severe hypoglycemia previously observed in other genetic mouse models of reduced GHSR signaling or hepatic GH action (24, 42, 48-53). Similarly, in GHSR-A203E mice, administered ghrelin-induced GH secretion was negligible, while GHRH-induced GH secretion was intact. These findings, in conjunction with increased GH protein content observed in pituitaries of GHSR-A203E mice and intact GHRH-induced GH release by GHSR-A203E mice, suggest a pattern of defective GH secretion resulting from defective signaling by the GHSR-A203E mutant.

Yet, the body weight phenotype of the GHSR-A203E mice did not match that attributed to the GHSR-A204E mutation in humans. As mentioned, several family members with the GHSR-A204E mutation and an unrelated GHSR-A204E carrier were shown to have overweight or

obesity (28, 29). However, in mice, the body weight curves of GHSR-A203E and wild-type littermates overlapped from 4 – 25 wks-of age, and eventually diverged with increasing age, such that by 65-66 wks-of-age, GHSR-A203E mice were ~19.7% lighter than wild-type mice. Supporting the development of reduced body weight in the aged GHSR-A203E mice, a subtle reduction in body weight gain was already apparent in the younger GHSR-A203E mice, as was a subtle reduction in cumulative feed efficiency (in males). Nonetheless, the younger GHSR-A203E mice exhibited increased food intake as compared to wild-type littermates. Notwithstanding the observation of overweight and obesity in many human GHSR-A204E carriers, the reduction in body weight observed in the GHSR-A203E mice fits better with the body weight phenotype expected upon reduced GHSR signaling. Our finding in mice suggests that the overweight and obesity phenotype of some human GHSR-A204E carriers is unrelated to the mutation (21).

Perhaps the greatest surprise of our current study relates to the seemingly discrepant observations of preserved ghrelin-dependent GHSR activity *in vitro* and *ex vivo* vs. absent or markedly reduced ghrelin-dependent GHSR activity *in vivo*. Specifically, baseline Gαq-mediated IP_3 accumulation was lower in COS-7 cells transfected with GHSR-A203E than in those transfected with GHSR-WT while ghrelin-induced IP_3 accumulation was observed in cells transfected with either construct. Also, basal reduction of $Ca_V2.2$ current density in $Ca_V2.2$-expressing HEK293T cells transfected with GHSR-WT was reversed by GHSR-A203E while ghrelin-induced inhibition of $Ca_V2.2$ current density was observed in cells transfected with either construct. These *in vitro* findings are similar to those observed previously for the human GHSR-A204E construct (10), and are further supported by our *ex vivo* evaluation of neurons from wild-type mice, GHSR-A203E mice, and GHSR-A203E-null mice: In cultured hypothalamic neurons from GHSR-A203E mice and GHSR-deficient mice, native calcium currents were increased as compared to wild-type mice, whereas in cultured hypothalamic neurons from GHSR-A203E mice and wild-type mice, ghrelin inhibited calcium currents. Also, in brain slices, resting membrane potentials of arcuate NPY neurons from GHSR-A203E mice were hyperpolarized as compared to those from wild-type mice, yet the same percentage of these neurons from GHSR-A203E and wild-type mice depolarized upon ghrelin exposure. As such, the *in vitro* and *ex vivo* studies clearly distinguished the effects of the A203E mutation on constitutive vs. ghrelin-dependent GHSR activity and, in so doing, demonstrated loss of constitutive GHSR activity but retained ghrelin-induced activity. Yet, the *in vivo* studies were not in agreement: Administered ghrelin exhibited absent orexigenic efficacy and markedly reduced GH secretagogue efficacy in GHSR-A203E mice. Parenthetically, it might be of interest in future studies to determine if the GHSR-A203E mice would respond more robustly to higher doses of administered ghrelin.

Thus, the *ex vivo* results support the conclusions that constitutive GHSR activity contributes to the native depolarizing conductance of GHSR-expressing arcuate NPY neurons and that the A203E mutation ablates constitutive GHSR activity (as those assessments were made in cells that normally express GHSR and in preparations without ghrelin). However, given the reduced responses to administered ghrelin *in vivo* in GHSR-A203E mice, it is uncertain whether the reduced body weight and body length observed in GHSR-A203E mice following the long-term feeding study or the exaggerated fall in blood glucose and markedly attenuated GH elevation observed in GHSR-A203E mice during the 7-d 60% caloric restriction study are due solely to loss of constitutive GHSR activity or also to deficient ghrelin-dependent GHSR activity. Indeed, the severe caloric restriction protocol was associated with an equivalently progressive increase in ghrelin over its week-long course in both GHSR-A203E and wild-type littermates.

There are several potential reasons for this discrepancy. First, *in vitro* studies are by nature artificial. As such, the effects on the signaling molecules studied may not represent the effects

on the actual signaling molecules that interact with GHSR within cells that express GHSR normally. Also, expression levels of wild-type GHSR or the GHSR-A203E mutant in the transfected cells may differ from those in cells that express GHSR normally. Additionally, expression levels of proteins that interact with GHSR, such as MRAP2 (melanocortin receptor accessory protein-2) may differ in transfected cells from those in native GHSR-expressing cells. MRAP2 affects GHSR activity in many ways and is required for ghrelin-induced food intake (54, 55). More specifically, MRAP2 potentiates ghrelin-dependent GHSR signaling via Gαq-mediated IP accumulation, inhibits constitutive GHSR signaling via Gαq, and decreases ghrelin-stimulated β-arrestin recruitment (54, 55). Also, co-transfection of CHO cells with human GHSR-A204E + MRAP2 markedly reduces ghrelin-dependent IP accumulation over that in cells transfected with GHSR-A204E alone (55). Thus, differential expression levels of MRAP2 in the COS-7 and HEK293T cells used here vs. those occurring naturally in cells that normally express GHSR could have contributed to the seemingly different results observed *in vitro* vs. *in vivo* for both GHSR-WT and GHSR-A203E. As another example, previous studies have revealed that GHSR forms heterodimers with other GPCRs, including MC3R, dopamine D1R, and dopamine D2R, among others (56-58). For instance, MC3R has been localized to most GHSR-expressing neurons in the arcuate nucleus (57). Co-transfection of COS-7 and HEK293 cells with both GHSR-WT + MC3R diminishes GHSR constitutive signaling and ghrelin-dependent GHSR signaling (57). Differential expression levels of heterodimer-forming GPCRs such as MC3R in transfected cells vs. naturally GHSR-expressing cells are undoubtedly present.

Second, focusing on one or two signaling systems in transfected cells, as we have done here, may not tell the whole story. For instance, in previous *in vitro* studies with the human GHSR-A204E mutant, while certain aspects of GHSR activity were preserved upon application of ghrelin (such as Gαq-mediated IP accumulation, as was also observed here using mouse GHSR-A203E), β-arrestin recruitment (which was reduced dramatically at baseline) could not be rescued by application of ghrelin (14). Additionally, the above-described heterodimerization of GHSR with other GPCRs also affects signaling via those other GPCRs. For instance, co-transfection of GHSR + MC3R enhances α-MSH signaling via MC3R-engaged, Gαs-mediated cAMP accumulation (57). Substitution of GHSR-A204E for wild-type GHSR leads to reduced α-MSH-induced cAMP accumulation (57). Thus, while our newly-reported effects of the GHSR-A203E mutation ± ghrelin on IP_3 accumulation and calcium currents *in vitro* suggest impaired constitutive GHSR activity and retained ghrelin-dependent GHSR activity, had additional signaling systems been tested, deficiencies in ghrelin-dependent GHSR activity may have been uncovered.

Third, while *ex vivo* systems avoid the artificial aspects of transfection studies, focusing on the activity of the GHSR-A203E mutation in only hypothalamic neurons, as we have done here, may miss effects of the mutation in other sites of GHSR expression. For example, ghrelin's orexigenic actions are distributed over several GHSR-expressing brain regions and neuronal cell types, including the caudal brainstem, midbrain, and hippocampus in addition to several hypothalamic nuclei (59-61). Different subsets of these regions and others are likely responsible to varying degrees for the ghrelin system's other actions (62). Ghrelin and the endogenous GHSR antagonist/inverse agonist LEAP2 may penetrate these different brain regions to varying degrees. As such, it is not necessarily the case that ghrelin-dependent and constitutive GHSR activity are engaged to the same relative degrees from one brain region to another or that ghrelin-dependent vs. constitutive GHSR activity are relevant in all brain regions.

5. Conclusions

In vitro, *ex vivo*, and *in vivo* methods were used to investigate the physiological significance of the GHSR-A203E mutation – a correlate of the naturally-occurring human GHSR-A204E mutation associated with a highly penetrant occurrence of short stature, GH deficiency and occasionally overweight or obesity. Our *in vitro* and *ex vivo* studies with mouse GHSR-A203E confirmed previous *in vitro* studies with a human GHSR-A204E construct, which demonstrated loss of constitutive GHSR activity but retained ghrelin-dependent GHSR activity. Reminiscent of the short stature and GH deficiency in human carriers, mice expressing GHSR-A203E instead of wild-type GHSR exhibited decreased body length and femur length when aged over one year, and defective GH secretion in response to a 7-d 60% caloric restriction protocol. Unlike human carriers who developed overweight and obesity, aged GHSR-A203E mice attained less body weight than wild-type littermates. Importantly, unlike the *in vitro* and *ex vivo* studies demonstrating retained ghrelin-dependent GHSR activity, GHSR-A203E mice exhibited a loss of administered ghrelin-induced food intake and a marked attenuation of administered ghrelin-induced GH release. Thus, based on our *ex vivo* studies, we can definitively state that constitutive GHSR activity contributes to native depolarizing conductance in arcuate NPY neurons. Also, based on our *in vivo* studies, we can definitively state that the GHSR-A203E mutation causes reduced body length, defective GH release, and diminished body weight. Yet, discrepancies in ghrelin-dependent GHSR-A203E activity as determined using the *in vitro* and *ex vivo* models vs. the *in vivo* model prevent us from attributing the phenotype of the GHSR-A203E mice – and, by extension, the phenotype of human carriers of the GHSR-A204E mutation – solely to defective constitutive GHSR activity.

6. Acknowledgments

This work was supported by the NIH (R01DK103884 to JZ), the Novo Nordisk Foundation Center for Basic Metabolic Research at the University of Copenhagen (to BH and JZ), and grants from the Fondo para la Investigación Científica y Tecnológica (PICT2016-1084 and PICT2017-3196 to MP and PICT2015-3330 and PICT2017- 0602) to JR). We would like to thank Dr. Guadalupe García Romero and Dr. Silvia Rodriguez (IMBICE) for their technical assistance, Drs. Diane Lipscombe, Jacky Marie, Silvia Rodriguez and Joel Elmquist for providing reagents, and the UT Southwestern Medical Center Transgenic Core Facility for their assistance in generating the GHSR-A203E mouse line.

Author contributions.

L.J.T., S.O.-L., J.R., Z.H., M.P.C., E.R.M., C.J., N.P., M.N., M.A.H., V.M.D., N.P.M., and B.K.M. performed the experiments, J.R., M.P., K.W.W., B.H., and J.M.Z. supervised the experiments, L.J.T., J.R., M.P., K.W.W., B.H., and J.M.Z. wrote the manuscript, and B.H. and J.M.Z. conceived of the study

7. Figure Legends

Figure 1: *In vitro* studies comparing signaling by GHSR-WT vs. GHSR-A203E mutant.
(A) Basal and ghrelin-induced IP_3 accumulation in COS-7 cells expressing GHSR-WT (EC_{50}=7.0 ± 0.8 X 10^{-9} M ; E_{max}= 99.3%) or GHSR-A203E (EC_{50}=1.7 ± 0.1 X 10^{-9} M; E_{max}= 88.7%) (n=5). Data were analyzed by an unpaired Student's t-test for 0, 10^{-6} and10^{-5} M concentrations of ghrelin. (B) Representative traces of Ca_V current and (C) mean Ca_V current values from HEK293T cells co-expressing $Ca_V2.2$ and its auxiliary subunits ($Ca_V\alpha_2\delta_1$ and $Ca_V\beta_3$) together with empty plasmid (Control, n=16) or GHSR-A203E (n=4) or GHSR-WT (n=4). Data were analyzed by Kruskal Wallis ANOVA followed by Dunn's post-hoc analysis. (D) Normalized representative traces of Ca_V current and (E) mean Ca_V current values from HEK293T cells co-expressing $Ca_V2.2$ and its auxiliary subunits ($Ca_V\alpha_2\delta_1$ and $Ca_V\beta_3$) together with GHSR-A203E (n=5) or GHSR-WT (n=5), in the absence and presence of ghrelin (500 nM). Data were analyzed by unpaired Student´s t-test. * P<0.05, **** P<0.0001, n.s.=non-significant.

Figure 2: Generation of the GHSR-A203E and GHSR-A203E-null mouse models.
(A) Schematic diagram of the derivation of the GHSR-A203E and GHSR-A203E-null mouse models by homologous recombination. (B) Hypothalamic expression of food intake- and body weight-related transcripts in 66 wk-old mice (n=7-9 per group). (C) Pituitary expression of GH secretion-related transcripts in 14 wk-old males (n=3 per group). Data were analyzed by unpaired Student's t-test. # P=0.051.

Figure 3: *Ex vivo* studies comparing native calcium current in cultured hypothalamic neurons from GHSR-A203E-null, wild-type, and GHSR-A203E mice.
(A) Representative traces of barium currents (I_{Ba}) and (B) mean I_{Ba} current values from cultured hypothalamic neurons from GHSR-A203E-null (n=16), wild-type (including a combination of wild-type littermates of both the GHSR-A203E-null and GHSR-A203E lines; n=10) and GHSR-A203E (n=25) mice. (C) Normalized representative traces of I_{Ba} currents and (D) mean I_{Ba} current values from hypothalamic neurons from GHSR-A203E-null (n=5), wild-type (n=4) and GHSR-A203E mice (n=11), in the absence and presence of ghrelin (500 nM). Data were analyzed by Kruskal Wallis ANOVA with Dunn's post-hoc analysis. * P<0.05, *** P<0.001, **** P<0.0001, n.s.=non-significant.

Figure 4: *Ex vivo* studies comparing electrophysiological properties of arcuate NPY neurons from wild-type vs. GHSR-A203E littermates.
(A) Representative NPY-GFP neuron from a wild-type mouse on an NPY-GFP background under (i) Brightfield illumination and (ii) FITC (GFP) illumination. Complete dialysis of Alexa Fluor 350 from the intracellular pipette is shown in (iii). A merged image of the targeted NPY neuron is shown in (iv). Arrow indicates the targeted cell. Scale bar = 50 µm. (B) Representative NPY-GFP neuron from a GHSR-A203E mouse on an NPY-GFP background under (i) Brightfield illumination and (ii) FITC (GFP) illumination. Complete dialysis of Alexa Fluor 594 from the intracellular pipette is shown in (iii). A merged image of the targeted NPY neuron is shown in (iv). Arrow indicates the targeted cell. Scale bars = 50 µm. (C, D) Representative Current-clamp recordings of NPY neurons from (C) wild-type and (D) GHSR-A203E mice, demonstrating resting membrane potentials and depolarization upon addition of ghrelin (100 nM). (E) Change of membrane potential in NPY neurons from wild-type or GHSR-A203E mice in response to ghrelin (100 nM) or vehicle (ACSF). Data were analyzed by 2-way ANOVA followed by a Tukey post-hoc analysis. ** P<0.01. (F-G) Linear regression analyses of current–voltage (I–V) plots of (F) wild-type (G) and GHSR-A203E mice.

Figure 5: Metabolic phenotype of wild-type and GHSR-A203E littermates.

(A-B) Body weight, (C-D) % weight gain, (E-F) food intake, (G-H) food intake/body weight, and (I-J) cumulative feed efficiency in male (A, C, E, G, and I) and female (B, D, F, H, and J) wild-type (n= 7-9) and GHSR-A203E (n=10-12) littermates. (K-L) Nose-anus body lengths in 26 wk-old male (K) (n=8-10) and 25 wk-old female (L) (n=9-12) mice. (M) Femur Length in 26 wk-old male (n=8-10) mice. Data were analyzed by (A-J) repeated measures 2-way ANOVA followed by a Tukey post hoc analysis or by (K-M) a Student's unpaired t-test. * P<0.05, *** P<0.001, **** P<0.0001, # 0.05≤P<0.1, n.s.=non-significant.

Figure 6: Metabolic effects of the GHSR-A203E mutation in older mice.
(A) Body weights of male mice aged 21-66 wks-of-age (n=7-10). (B) Body lengths of male mice at 3 different ages (n=7-9). (C) Femur lengths of male mice at 65-66 weeks-of-age (n=6-8). Data were analyzed by (A-B) repeated measures 2-way ANOVA followed by a Sidak's Multiple Comparison post-hoc analysis or by (C) an unpaired Student's t-test. * P<0.05, **** P<0.0001.

Figure 7: *In vivo* effects of administered ghrelin in wild-type and GHSR-A203E littermates.
(A) Ghrelin [0 (saline), 0.1, and 1 mg/kg s.c.)-induced 2-h food intake in 25-week-old male mice (n=7-10). (B-C) Ghrelin (2 mg/kg s.c.)-induced (B) 2-h food intake and RER (2-h after ghrelin administration) in 9-12-week-old male mice (n=6-7). (D) Ghrelin (0.5 mg/kg i.p.)-induced GH secretion in 7-week-old mice (n=3-4). (E) GHRH (0.5 mg/kg i.p.)-induced GH secretion in 10-week-old mice (n=7). (F) Plasma IGF-1 (n=6-8) and (G) pituitary GH content (n=5-8) in 66-week-old mice. Data were analyzed by (A) a 2-way ANOVA followed by a Tukey post-hoc analysis, (B-E) a 2-way repeated measures ANOVA followed by a Sidak's Multiple Comparison post-hoc analysis, or (F-G) an unpaired Student's t-test. * P<0.05, ** P<0.01, **** P<0.0001, # 0.05≤P<0.1, n.s.=non-significant.

Figure 8: Effects of a 7-d severe (60%) caloric restriction protocol
(A) Body weights, (B) % fat mass, (C) % lean mass (n=9-20), (D) plasma GH levels (n=7-10), (E) plasma ghrelin (n=7-13), (F) blood glucose (n=9-20), and (G) % survival (9/9 wild-type mice and 17/20 GHSR-A203E mice) over the 7-d course of daily access to 40% of usual daily calories. (A-F) Data were analyzed by 2-way ANOVA followed by Tukey post-hoc analyses. (G) Survival curves were calculated by the Kaplan-Meier method, with comparisons determined using the Mantel-Cox log-rank test. * P<0.05, **** P<0.0001, n.s.=non-significant.

8. References

[1] Kojima, M., Hosoda, H., Date, Y., Nakazato, M., Matsuo, H., and Kangawa, K. 1999. Ghrelin is a growth-hormone-releasing acylated peptide from stomach. *Nature* 402:656-660.

[2] Mani, B.K., and Zigman, J.M. 2017. Ghrelin as a Survival Hormone. *Trends Endocrinol Metab* 28:843-854.

[3] Muller, T.D., Nogueiras, R., Andermann, M.L., Andrews, Z.B., Anker, S.D., Argente, J., Batterham, R.L., Benoit, S.C., Bowers, C.Y., Broglio, F., et al. 2015. Ghrelin. *Mol Metab* 4:437-460.

[4] Holst, B., and Schwartz, T.W. 2004. Constitutive ghrelin receptor activity as a signaling set-point in appetite regulation. *Trends Pharmacol Sci* 25:113-117.

[5] Edwards, A., and Abizaid, A. 2017. Clarifying the Ghrelin System's Ability to Regulate Feeding Behaviours Despite Enigmatic Spatial Separation of the GHSR and Its Endogenous Ligand. *Int J Mol Sci* 18.

[6] Schalla, M.A., and Stengel, A. 2019. Pharmacological Modulation of Ghrelin to Induce Weight Loss: Successes and Challenges. *Curr Diab Rep* 19:102.

[7] Mear, Y., Enjalbert, A., and Thirion, S. 2013. GHS-R1a constitutive activity and its physiological relevance. *Front Neurosci* 7:87.

[8] Holst, B., Cygankiewicz, A., Jensen, T.H., Ankersen, M., and Schwartz, T.W. 2003. High constitutive signaling of the ghrelin receptor--identification of a potent inverse agonist. *Mol Endocrinol* 17:2201-2210.

[9] Liu, G., Fortin, J.P., Beinborn, M., and Kopin, A.S. 2007. Four missense mutations in the ghrelin receptor result in distinct pharmacological abnormalities. *J Pharmacol Exp Ther* 322:1036-1043.

[10] Lopez Soto, E.J., Agosti, F., Cabral, A., Mustafa, E.R., Damonte, V.M., Gandini, M.A., Rodriguez, S., Castrogiovanni, D., Felix, R., Perello, M., et al. 2015. Constitutive and ghrelin-dependent GHSR1a activation impairs CaV2.1 and CaV2.2 currents in hypothalamic neurons. *J Gen Physiol* 146:205-219.

[11] Mustafa, E.R., Lopez Soto, E.J., Martinez Damonte, V., Rodriguez, S.S., Lipscombe, D., and Raingo, J. 2017. Constitutive activity of the Ghrelin receptor reduces surface expression of voltage-gated Ca(2+) channels in a CaVbeta-dependent manner. *J Cell Sci* 130:3907-3917.

[12] Ramirez, V.T., van Oeffelen, W., Torres-Fuentes, C., Chruscicka, B., Druelle, C., Golubeva, A.V., van de Wouw, M., Dinan, T.G., Cryan, J.F., and Schellekens, H. 2019. Differential functional selectivity and downstream signaling bias of ghrelin receptor antagonists and inverse agonists. *FASEB J* 33:518-531.

[13] Holst, B., Holliday, N.D., Bach, A., Elling, C.E., Cox, H.M., and Schwartz, T.W. 2004. Common Structural Basis for Constitutive Activity of the Ghrelin Receptor Family. *J Biol Chem* 279:53806-53817.

[14] Mokrosinski, J., Frimurer, T.M., Sivertsen, B., Schwartz, T.W., and Holst, B. 2012. Modulation of constitutive activity and signaling bias of the ghrelin receptor by conformational constraint in the second extracellular loop. *J Biol Chem* 287:33488-33502.

[15] Petersen, P.S., Woldbye, D.P., Madsen, A.N., Egerod, K.L., Jin, C., Lang, M., Rasmussen, M., Beck-Sickinger, A.G., and Holst, B. 2009. In vivo characterization of high Basal signaling from the ghrelin receptor. *Endocrinology* 150:4920-4930.

[16] Kemp, B.A., Howell, N.L., Gildea, J.J., and Padia, S.H. 2014. Intrarenal ghrelin receptor antagonism prevents high-fat diet-induced hypertension in male rats. *Endocrinology* 155:2658-2666.

[17] Fernandez, G., Cabral, A., Andreoli, M.F., Labarthe, A., M'Kadmi, C., Ramos, J.G., Marie, J., Fehrentz, J.A., Epelbaum, J., Tolle, V., et al. 2018. Evidence Supporting a Role for Constitutive Ghrelin Receptor Signaling in Fasting-Induced Hyperphagia in Male Mice. *Endocrinology* 159:1021-1034.

[18] Cornejo, M.P., Castrogiovanni, D., Schioth, H.B., Reynaldo, M., Marie, J., Fehrentz, J.A., and Perello, M. 2019. Growth hormone secretagogue receptor signalling affects high-fat intake independently of plasma levels of ghrelin and LEAP2, in a 4-day binge eating model. *J Neuroendocrinol* 31:e12785.

[19] Abegg, K., Bernasconi, L., Hutter, M., Whiting, L., Pietra, C., Giuliano, C., Lutz, T.A., and Riediger, T. 2017. Ghrelin receptor inverse agonists as a novel therapeutic approach against obesity-related metabolic disease. *Diabetes Obes Metab* 19:1740-1750.

[20] Denney, W.S., Sonnenberg, G.E., Carvajal-Gonzalez, S., Tuthill, T., and Jackson, V.M. 2017. Pharmacokinetics and pharmacodynamics of PF-05190457: The first oral ghrelin receptor inverse agonist to be profiled in healthy subjects. *Br J Clin Pharmacol* 83:326-338.

[21] Holst, B., and Schwartz, T.W. 2006. Ghrelin receptor mutations--too little height and too much hunger. *J Clin Invest* 116:637-641.

[22] Chan, C.B., Leung, P.K., Wise, H., and Cheng, C.H. 2004. Signal transduction mechanism of the seabream growth hormone secretagogue receptor. *FEBS Lett* 577:147-153.

[23] Mende, F., Hundahl, C., Plouffe, B., Skov, L.J., Sivertsen, B., Madsen, A.N., Luckmann, M., Diep, T.A., Offermanns, S., Frimurer, T.M., et al. 2018. Translating biased signaling in the ghrelin receptor system into differential in vivo functions. *Proc Natl Acad Sci U S A* 115:E10255-E10264.

[24] Ge, X., Yang, H., Bednarek, M.A., Galon-Tilleman, H., Chen, P., Chen, M., Lichtman, J.S., Wang, Y., Dalmas, O., Yin, Y., et al. 2018. LEAP2 Is an Endogenous Antagonist of the Ghrelin Receptor. *Cell Metab* 27:461-469 e466.

[25] M'Kadmi, C., Cabral, A., Barrile, F., Giribaldi, J., Cantel, S., Damian, M., Mary, S., Denoyelle, S., Dutertre, S., Peraldi-Roux, S., et al. 2019. N-Terminal Liver-Expressed Antimicrobial Peptide 2 (LEAP2) Region Exhibits Inverse Agonist Activity toward the Ghrelin Receptor. *J Med Chem* 62:965-973.

[26] Mani, B.K., Puzziferri, N., He, Z., Rodriguez, J.A., Osborne-Lawrence, S., Metzger, N.P., Chhina, N., Gaylinn, B., Thorner, M.O., Thomas, E.L., et al. 2019. LEAP2 changes with body mass and food intake in humans and mice. *J Clin Invest* 129:3909-3923.

[27] Barrile, F., M'Kadmi, C., De Francesco, P.N., Cabral, A., Garcia Romero, G., Mustafa, E.R., Cantel, S., Damian, M., Mary, S., Denoyelle, S., et al. 2019. Development of a novel fluorescent ligand of growth hormone secretagogue receptor based on the N-Terminal Leap2 region. *Mol Cell Endocrinol* 498:110573.

[28] Pantel, J., Legendre, M., Cabrol, S., Hilal, L., Hajaji, Y., Morisset, S., Nivot, S., Vie-Luton, M.P., Grouselle, D., de Kerdanet, M., et al. 2006. Loss of constitutive activity of the growth hormone secretagogue receptor in familial short stature. *J Clin Invest* 116:760-768.

[29] Wang, H.J., Geller, F., Dempfle, A., Schauble, N., Friedel, S., Lichtner, P., Fontenla-Horro, F., Wudy, S., Hagemann, S., Gortner, L., et al. 2004. Ghrelin receptor gene: identification of several sequence variants in extremely obese children and adolescents, healthy normal-weight and underweight students, and children with short normal stature. *J Clin Endocrinol Metab* 89:157-162.

[30] Inoue, H., Kangawa, N., Kinouchi, A., Sakamoto, Y., Kimura, C., Horikawa, R., Shigematsu, Y., Itakura, M., Ogata, T., Fujieda, K., et al. 2011. Identification and functional analysis of novel human growth hormone secretagogue receptor (GHSR)

gene mutations in Japanese subjects with short stature. *J Clin Endocrinol Metab* 96:E373-378.

[31] Sivertsen, B., Lang, M., Frimurer, T.M., Holliday, N.D., Bach, A., Els, S., Engelstoft, M.S., Petersen, P.S., Madsen, A.N., Schwartz, T.W., et al. 2011. Unique interaction pattern for a functionally biased ghrelin receptor agonist. *J Biol Chem* 286:20845-20860.

[32] Thaler, C., Gray, A.C., and Lipscombe, D. 2004. Cumulative inactivation of N-type CaV2.2 calcium channels modified by alternative splicing. *Proc Natl Acad Sci U S A* 101:5675-5679.

[33] Zigman, J.M., Nakano, Y., Coppari, R., Balthasar, N., Marcus, J.N., Lee, C.E., Jones, J.E., Deysher, A.E., Waxman, A.R., White, R.D., et al. 2005. Mice lacking ghrelin receptors resist the development of diet-induced obesity. *J Clin Invest* 115:3564-3572.

[34] Lewandoski, M., Wassarman, K.M., and Martin, G.R. 1997. Zp3-cre, a transgenic mouse line for the activation or inactivation of loxP-flanked target genes specifically in the female germ line. *Curr Biol* 7:148-151.

[35] Martinez Damonte, V., Rodriguez, S.S., and Raingo, J. 2018. Growth hormone secretagogue receptor constitutive activity impairs voltage-gated calcium channel-dependent inhibitory neurotransmission in hippocampal neurons. *J Physiol* 596:5415-5428.

[36] Raingo, J., Castiglioni, A.J., and Lipscombe, D. 2007. Alternative splicing controls G protein-dependent inhibition of N-type calcium channels in nociceptors. *Nat Neurosci* 10:285-292.

[37] van den Pol, A.N., Yao, Y., Fu, L.Y., Foo, K., Huang, H., Coppari, R., Lowell, B.B., and Broberger, C. 2009. Neuromedin B and gastrin-releasing peptide excite arcuate nucleus neuropeptide Y neurons in a novel transgenic mouse expressing strong Renilla green fluorescent protein in NPY neurons. *J Neurosci* 29:4622-4639.

[38] Williams, K.W., Liu, T., Kong, X., Fukuda, M., Deng, Y., Berglund, E.D., Deng, Z., Gao, Y., Liu, T., Sohn, J.W., et al. 2014. Xbp1s in Pomc neurons connects ER stress with energy balance and glucose homeostasis. *Cell Metab* 20:471-482.

[39] He, Z., Gao, Y., Alhadeff, A.L., Castorena, C.M., Huang, Y., Lieu, L., Afrin, S., Sun, J., Betley, J.N., Guo, H., et al. 2018. Cellular and synaptic reorganization of arcuate NPY/AgRP and POMC neurons after exercise. *Mol Metab* 18:107-119.

[40] Sun, Y., Wang, P., Zheng, H., and Smith, R.G. 2004. Ghrelin stimulation of growth hormone release and appetite is mediated through the growth hormone secretagogue receptor. *Proc Natl Acad Sci U S A* 101:4679-4684.

[41] Holst, B., Madsen, K.L., Jansen, A.M., Jin, C., Rickhag, M., Lund, V.K., Jensen, M., Bhatia, V., Sorensen, G., Madsen, A.N., et al. 2013. PICK1 deficiency impairs secretory vesicle biogenesis and leads to growth retardation and decreased glucose tolerance. *PLoS Biol* 11:e1001542.

[42] Mani, B.K., Osborne-Lawrence, S., Vijayaraghavan, P., Hepler, C., and Zigman, J.M. 2016. beta1-Adrenergic receptor deficiency in ghrelin-expressing cells causes hypoglycemia in susceptible individuals. *J Clin Invest* 126:3467-3478.

[43] Cowley, M.A., Smith, R.G., Diano, S., Tschop, M., Pronchuk, N., Grove, K.L., Strasburger, C.J., Bidlingmaier, M., Esterman, M., Heiman, M.L., et al. 2003. The distribution and mechanism of action of ghrelin in the CNS demonstrates a novel hypothalamic circuit regulating energy homeostasis. *Neuron* 37:649-661.

[44] Zigman, J.M., Jones, J.E., Lee, C.E., Saper, C.B., and Elmquist, J.K. 2006. Expression of ghrelin receptor mRNA in the rat and the mouse brain. *J Comp Neurol* 494:528-548.

[45] Huang, Y., He, Z., Gao, Y., Lieu, L., Yao, T., Sun, J., Liu, T., Javadi, C., Box, M., Afrin, S., et al. 2018. PI3K is integral for the acute activity of leptin and insulin in arcuate NPY/AgRP neurons in males. *Journal of the Endocrine Society*:js.2018-00061-js.02018-00061.

[46] Purves, D. 2008. *Neuroscience*. Sunderland, Mass.: Sinauer. xvii, 857, G-816, IC-857, I-829 p. pp.
[47] Kandel, E.R. 2013. *Principles of neural science*. New York: McGraw-Hill. l, 1709 p. pp.
[48] Zhao, T.J., Liang, G., Li, R.L., Xie, X., Sleeman, M.W., Murphy, A.J., Valenzuela, D.M., Yancopoulos, G.D., Goldstein, J.L., and Brown, M.S. 2010. Ghrelin O-acyltransferase (GOAT) is essential for growth hormone-mediated survival of calorie-restricted mice. *Proc Natl Acad Sci U S A* 107:7467-7472.
[49] Li, R.L., Sherbet, D.P., Elsbernd, B.L., Goldstein, J.L., Brown, M.S., and Zhao, T.J. 2012. Profound hypoglycemia in starved, ghrelin-deficient mice is caused by decreased gluconeogenesis and reversed by lactate or fatty acids. *J Biol Chem*.
[50] McFarlane, M.R., Brown, M.S., Goldstein, J.L., and Zhao, T.J. 2014. Induced ablation of ghrelin cells in adult mice does not decrease food intake, body weight, or response to high-fat diet. *Cell Metab* 20:54-60.
[51] Zhang, Y., Fang, F., Goldstein, J.L., Brown, M.S., and Zhao, T.J. 2015. Reduced autophagy in livers of fasted, fat-depleted, ghrelin-deficient mice: reversal by growth hormone. *Proc Natl Acad Sci U S A* 112:1226-1231.
[52] Fang, F., Shi, X., Brown, M.S., Goldstein, J.L., and Liang, G. 2019. Growth hormone acts on liver to stimulate autophagy, support glucose production, and preserve blood glucose in chronically starved mice. *Proc Natl Acad Sci U S A* 116:7449-7454.
[53] Wang, Q., Liu, C., Uchida, A., Chuang, J.C., Walker, A., Liu, T., Osborne-Lawrence, S., Mason, B.L., Mosher, C., Berglund, E.D., et al. 2014. Arcuate AgRP neurons mediate orexigenic and glucoregulatory actions of ghrelin. *Mol Metab* 3:64-72.
[54] Srisai, D., Yin, T.C., Lee, A.A., Rouault, A.A.J., Pearson, N.A., Grobe, J.L., and Sebag, J.A. 2017. MRAP2 regulates ghrelin receptor signaling and hunger sensing. *Nat Commun* 8:713.
[55] Rouault, A.A.J., Rosselli-Murai, L.K., Hernandez, C.C., Gimenez, L.E., Tall, G.G., and Sebag, J.A. 2020. The GPCR accessory protein MRAP2 regulates both biased signaling and constitutive activity of the ghrelin receptor GHSR1a. *Sci Signal* 13.
[56] Kern, A., Albarran-Zeckler, R., Walsh, H.E., and Smith, R.G. 2012. Apo-ghrelin receptor forms heteromers with DRD2 in hypothalamic neurons and is essential for anorexigenic effects of DRD2 agonism. *Neuron* 73:317-332.
[57] Rediger, A., Piechowski, C.L., Yi, C.X., Tarnow, P., Strotmann, R., Gruters, A., Krude, H., Schoneberg, T., Tschop, M.H., Kleinau, G., et al. 2011. Mutually opposite signal modulation by hypothalamic heterodimerization of ghrelin and melanocortin-3 receptors. *J Biol Chem* 286:39623-39631.
[58] Schellekens, H., van Oeffelen, W.E., Dinan, T.G., and Cryan, J.F. 2013. Promiscuous dimerization of the growth hormone secretagogue receptor (GHS-R1a) attenuates ghrelin-mediated signaling. *J Biol Chem* 288:181-191.
[59] Kanoski, S.E., Fortin, S.M., Ricks, K.M., and Grill, H.J. 2013. Ghrelin signaling in the ventral hippocampus stimulates learned and motivational aspects of feeding via PI3K-Akt signaling. *Biol Psychiatry* 73:915-923.
[60] Abizaid, A., Liu, Z.W., Andrews, Z.B., Shanabrough, M., Borok, E., Elsworth, J.D., Roth, R.H., Sleeman, M.W., Picciotto, M.R., Tschop, M.H., et al. 2006. Ghrelin modulates the activity and synaptic input organization of midbrain dopamine neurons while promoting appetite. *J Clin Invest* 116:3229-3239.
[61] Faulconbridge, L.F., Grill, H.J., Kaplan, J.M., and Daniels, D. 2008. Caudal brainstem delivery of ghrelin induces fos expression in the nucleus of the solitary tract, but not in the arcuate or paraventricular nuclei of the hypothalamus. *Brain Res* 1218:151-157.
[62] Chuang, J.C., Perello, M., Sakata, I., Osborne-Lawrence, S., Savitt, J.M., Lutter, M., and Zigman, J.M. 2011. Ghrelin mediates stress-induced food-reward behavior in mice. *J Clin Invest* 121:2684-2692.

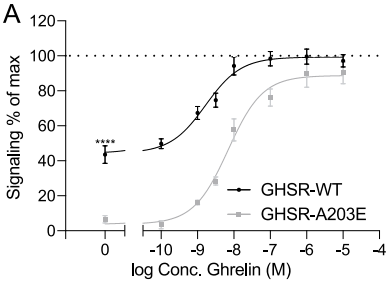

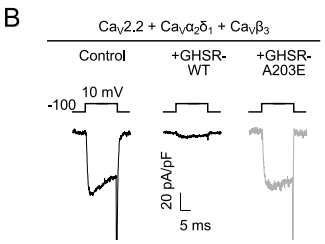

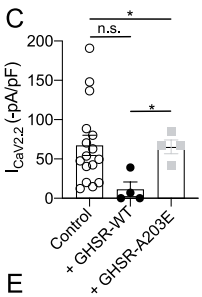

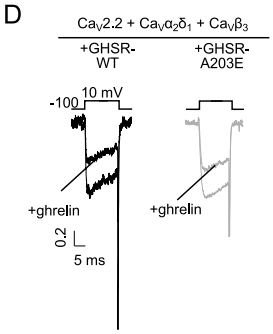

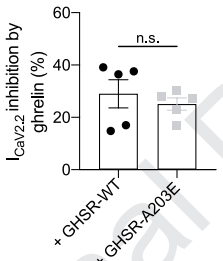

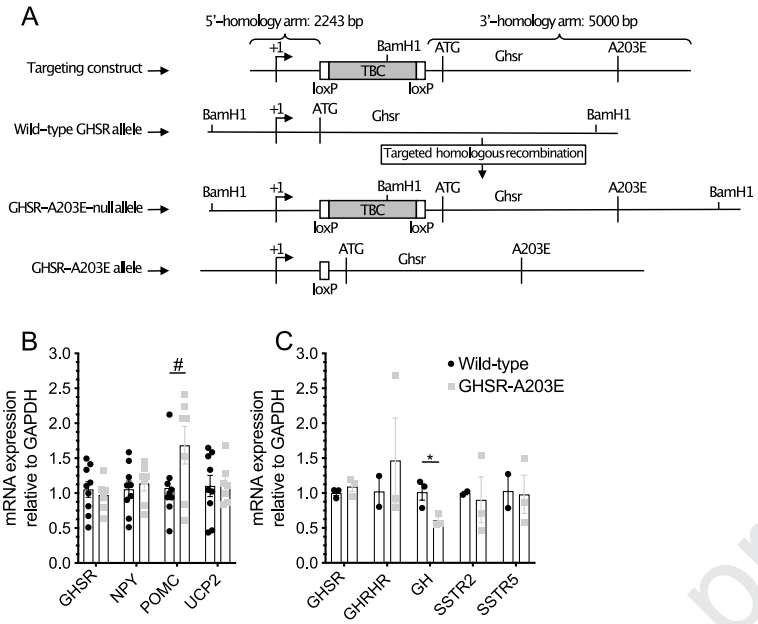

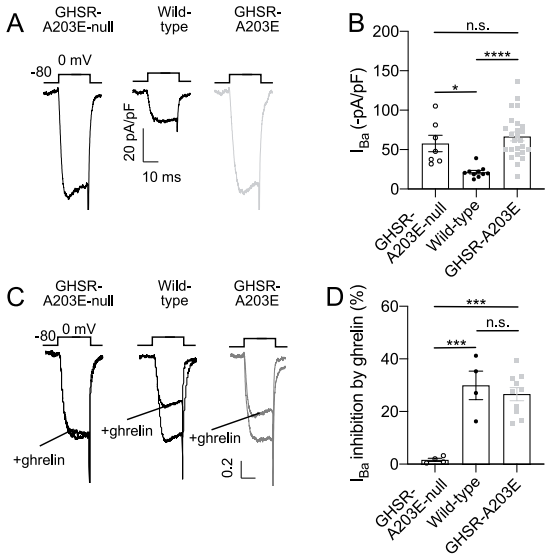

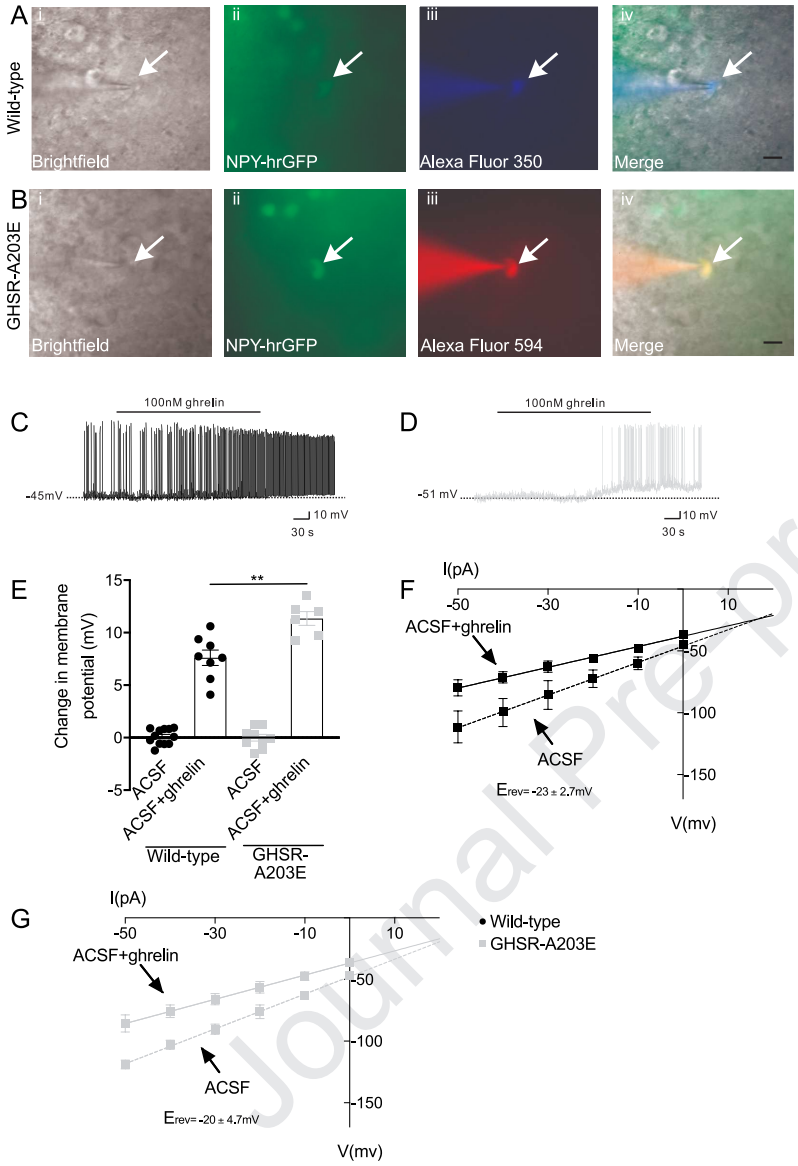

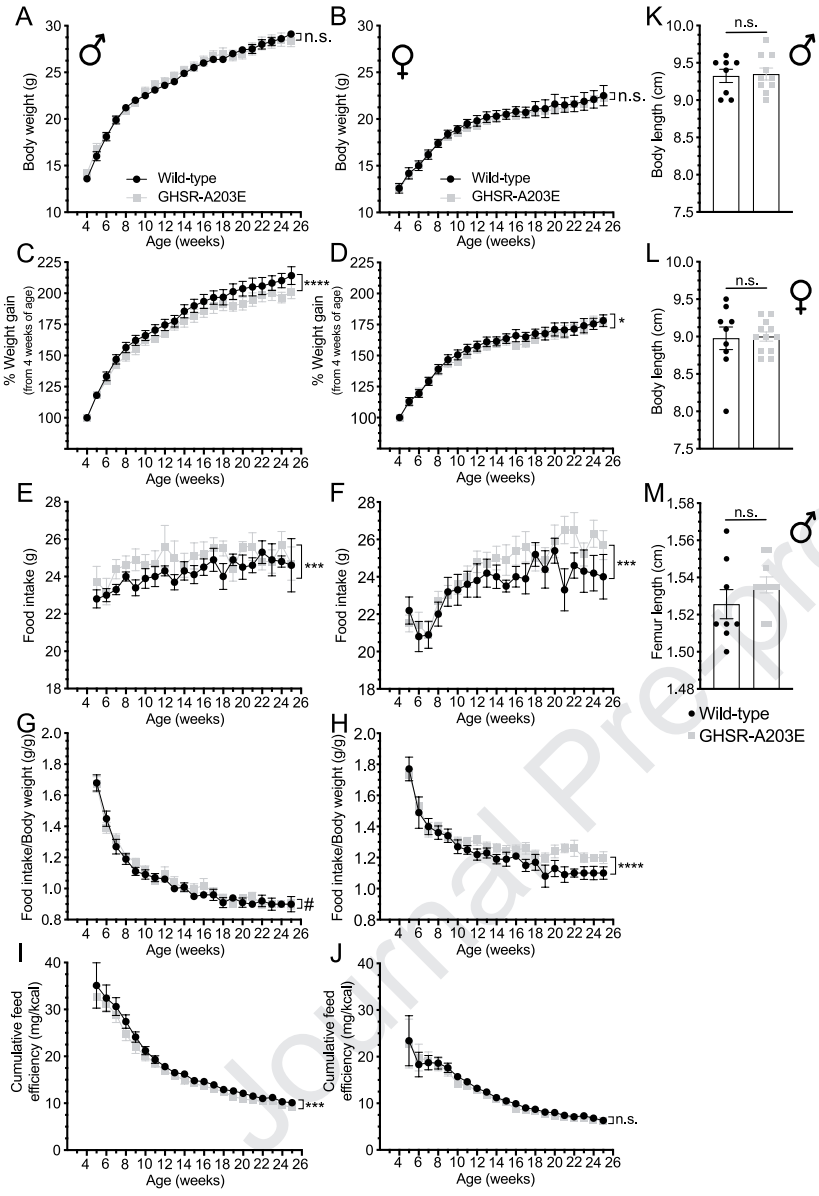

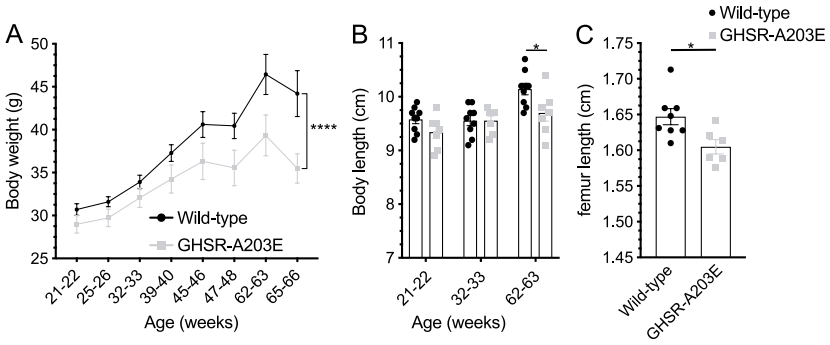

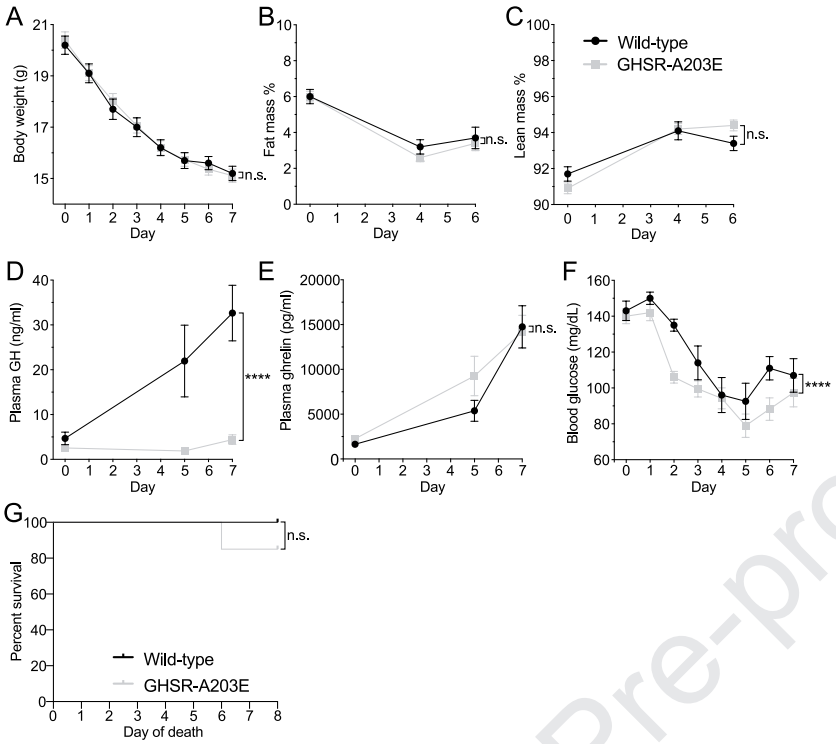

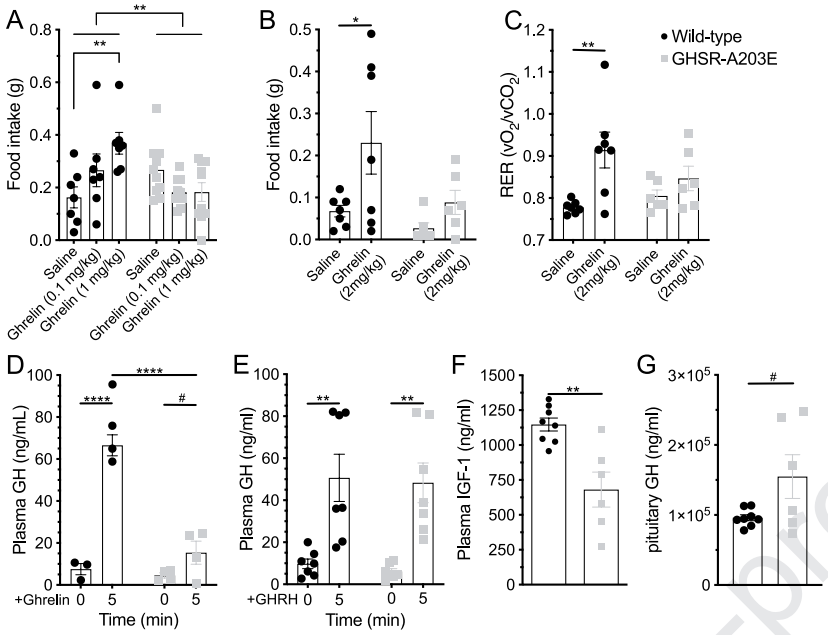

Highlights

- We generated mice with a GHSR mutation replacing Ala at position 203 with Glu
- The A203E mutation ablates constitutive GHSR activity & hyperpolarizes NPY neurons
- GHSR-A203E mice lack the usual orexigenic response to administered ghrelin
- The GHSR-A203E mutation blunts GH release and causes reduced body length
- This is consistent with short stature in human carriers of the GHSR-A204E mutation

The authors report nothing to disclose.